R1 correction in amide proton transfer imaging: Indication of the influence of transcytolemmal water exchange on CEST measurements

ARTICLE *in* NMR IN BIOMEDICINE · OCTOBER 2015

Impact Factor: 3.04 · DOI: 10.1002/nbm.3428

9 AUTHORS, INCLUDING:

Hua Li

Vanderbilt University

15 PUBLICATIONS **59** CITATIONS

SEE PROFILE

Xiaoyu Jiang

Vanderbilt University

12 PUBLICATIONS **51** CITATIONS

SEE PROFILE

Zhongliang Zu

Vanderbilt University

21 PUBLICATIONS **205** CITATIONS

SEE PROFILE

Junzhong Xu

Vanderbilt University

31 PUBLICATIONS **343** CITATIONS

SEE PROFILE

Research article

NMR IN BIOMEDICINE

Received: 8 April 2015, Revised: 26 August 2015, Accepted: 11 September 2015, Published online in Wiley Online Library

(wileyonlinelibrary.com) DOI: 10.1002/nbm.3428

R_1 correction in amide proton transfer imaging: indication of the influence of transcytolemmal water exchange on CEST measurements

Hua Li[a,b], Ke Li[a,c], Xiao-Yong Zhang[a,c], Xiaoyu Jiang[a,c], Zhongliang Zu[a,c], Moritz Zaiss[d], Daniel F. Gochberg[a,b,c], John C. Gore[a,b,c,e,f] and Junzhong Xu[a,b,c]*

Amide proton transfer (APT) imaging may potentially detect mobile proteins/peptides non-invasively *in vivo*, but its specificity may be reduced by contamination from other confounding effects such as asymmetry of non-specific magnetization transfer (MT) effects and spin–lattice relaxation with rate R_1 (=1/T_1). Previously reported spillover, MT and R_1 correction methods were based on a two-pool model, in which the existence of multiple water compartments with heterogeneous relaxation properties in real tissues was ignored. Such simple models may not adequately represent real tissues, and thus such corrections may be unreliable. The current study investigated the effectiveness and accuracy of correcting for R_1 in APT imaging via simulations and *in vivo* experiments using tumor-bearing rats subjected to serial injections of Gd-DTPA that produced different tissue R_1 values in regions of blood–brain-barrier breakdown. The results suggest that conventional measurements of APT contrast (such as APT* and MTR_{asym}) may be significantly contaminated by R_1 variations, while the R_1-corrected metric AREX* was found to be relatively unaffected by R_1 changes over a broad range (0.4–1 Hz). Our results confirm the importance of correcting for spin–lattice relaxation effects in quantitative APT imaging, and demonstrate the reliability of using the observed tissue R_1 for corrections to obtain more specific and accurate measurements of APT contrast *in vivo*. The results also indicate that, due to relatively fast transcytolemmal water exchange, the influence of intra- and extracellular water compartments on CEST measurements with seconds long saturation time may be ignored in tumors. Copyright © 2015 John Wiley & Sons, Ltd.

Keywords: R_1; APT; CEST; AREX; Gd-DTPA; tumor; transcytolemmal water exchange

INTRODUCTION

Chemical exchange saturation transfer (CEST) imaging can measure the concentrations of relatively small solutes indirectly by detecting the attenuation of water signals induced by chemical exchange (1,2). Compared with direct MR measurements (e.g. using high resolution MRS) of pools of solute protons at low concentrations (typically millimolar or lower) in biological tissues, the detection of changes in the background water signal caused by saturation transfer significantly enhances the sensitivity (by up to 500 000 (3)) for detecting low levels of exchanging compounds. Thus CEST provides an attractive means to image distributions of molecules such as peptides and metabolites with potentially

* *Correspondence to: J. Xu, Institute of Imaging Science, Vanderbilt University, Nashville, TN, USA.*
E-mail: junzhong.xu@vanderbilt.edu

a *H. Li, K. Li, X.-Y. Zhang, X. Jiang, Z. Zu, D. F. Gochberg, J. C. Gore, J. Xu*
Institute of Imaging Science, Vanderbilt University, Nashville, TN, USA

b *H. Li, D. F. Gochberg, J. C. Gore, J. Xu*
Department of Physics and Astronomy, Vanderbilt University, Nashville, TN, USA

c *K. Li, X.-Y. Zhang, X. Jiang, Z. Zu, D. F. Gochberg, J. C. Gore, J. Xu*
Department of Radiology and Radiological Sciences, Vanderbilt University, Nashville, TN, USA

d *M. Zaiss*
Department of Medical Physics in Radiology, Deutsches Krebsforschungszentrum (DKFZ, German Cancer Research Center), Heidelberg, Germany

e *J. C. Gore*
Department of Biomedical Engineering, Vanderbilt University, Nashville, TN, USA

f *J. C. Gore*
Department of Molecular Physiology and Biophysics, Vanderbilt University, Nashville, TN, USA

Abbreviations used: *CEST, chemical exchange saturation transfer; APT, amide proton transfer; MT, magnetization transfer; MTR_{asym}, magnetization transfer ratio obtained using asymmetric analysis; NOE, nuclear Overhauser effect; APT*, amide proton transfer obtained using the three-offset method; AREX, apparent exchange-dependent relaxation obtained using the 1/Z method; AREX*, AREX obtained using the 1/Z method and three-offset method; k_{AB}, transcytolemmal exchange rate from intra- to extracellular spaces; SPGR, spoiled-gradient echo; ROI, region of interest; APTR, proton transfer ratio for amide protons; NOER, NOE-based MT ratio.*

higher signal-to-noise ratios and higher spatial resolutions. During CEST experiments, saturated water signals ($M_{sat}(\Delta\omega)$) are usually acquired over a range of irradiation offset frequencies ($\Delta\omega$) around the water resonance and normalized by the corresponding unsaturated water signal M_0. The Z-spectrum ($Z(\Delta\omega) = M_{sat}(\Delta\omega)/M_0$) is then used to quantify the CEST contrast at different offsets. Amide proton transfer (APT), a specific form of CEST at $\Delta\omega$ = 3.6 ppm relative to water, has been suggested as a surrogate biomarker of endogenous mobile proteins and peptides as well as a pH-dependent indicator of amide proton exchange rates in biological tissues. APT has been widely implemented for characterizing abnormal tissues such as tumors (3–6) and stroke (7–10).

Unfortunately, APT imaging in practice may be significantly influenced by factors other than chemical exchange, including effects caused by B_0 inhomogeneities, non-specific magnetization transfer (MT) and asymmetric MT effects, water longitudinal relaxation rate (R_1), and direct water saturation (RF spillover). Several approaches have been developed to reduce these confounding effects. For example, the WASSR method corrects for spatial B_0 field variations (11). The magnetization transfer asymmetry (MTR_{asym}) metric corrects for direct water saturation by subtracting the signals acquired with irradiation on the solute of interest (the label scan) from those on the other side of water (the reference scan). However, in most biological tissues the background MT effects are themselves asymmetric, and nuclear Overhauser effects (NOEs) also can contribute, so MTR_{asym} is still influenced by processes that are not specific for chemical exchange of amides. These significantly reduce the specificity and quantitative accuracy of APT for detecting and measuring mobile proteins/peptides, and complicate the interpretation of APT data. Furthermore, MTR_{asym} makes no correction for R_1 contributions.

Several refinements have been proposed to further reduce the effects of asymmetric MT (12–16). For example, Jin *et al.* proposed to exploit the wide spectral separation available at high field strength (e.g. 9.4 T) and interpolate measurements made at three offset frequencies to better approximate APT, denoted as APT* (16). Different acquisition strategies, such as SAFARI (13), CERT (17), and VDMP-CEST (15), have also been developed to eliminate some confounding effects. However, these methods (like MTR_{asym}) do not incorporate a correction for R_1 effects on CEST measurements. Recently, Zaiss *et al.* analyzed the behaviors of CEST measurements and developed a reciprocal Z-spectrum analysis (denoted as the 1/Z method) to eliminate RF spillover and MT effects (18–20). Moreover, this analysis indicates a simple way in which the influence of R_1 on APT measurements can be eliminated. By combining the three-offset and the 1/Z methods, a new metric, AREX* (apparent exchange-dependent relaxation), can be obtained, which is an exchange-rate-weighted APT contrast with much reduced influence from other confounding effects. This method has been successfully implemented to characterize brain cancer in rats (21) and humans (22), and stroke in rats (19,23), resulting in very different estimates of APT effects compared with more conventional methods such as MTR_{asym} and APT*. These results suggest strongly that the influence of R_1 plays an important role in estimates of APT contrast.

Like most other CEST models, the 1/Z analysis was originally developed based on a simple two-pool (water and amide protons) model, in which a single, measured average R_1 of water is used in corrections (19,21,23,24). Although a recent study extended the 1/Z method to a three-pool model to include the semi-solid MT pool (25), the complex arrangement of multiple water pools in real biological tissues is still not considered. It is well known that water may exist in multiple compartments, such as intra- and extracellular spaces, and the relaxation properties in each compartment are likely different from each other. Moreover, not all pools necessarily have large numbers of exchanging protons, so the assumption of a single relaxation rate to represent all pools may introduce inaccuracies, especially if the water compartment fractions and relaxation rates change in pathologies such as stroke (26). There are therefore reasons to question whether R_1 correction approaches based on simple two-pool models are appropriate, and whether they can introduce extra uncertainty into estimates of APT effects.

In principle, the potentially confounding influences of water compartmentation and heterogeneous relaxation in real tissues on APT measurements may be significantly reduced if transcytolemmal water exchange occurs rapidly compared with the long (several seconds) duration of the saturation phase. For example, the apparent mean lifetime of intracellular water has been reported as 625 ± 43 ms in human frontal white matter and 344.8 ± 95.1 ms in human solid brain tumors (27). Moreover, the apparent mean lifetime of intracellular water in tumors can decrease further to 147 ± 84 ms during apoptosis (28). For a comparison, the total duration of saturation pulse (s) is of the order of several seconds, many times larger than the typical intracellular water lifetime. If the water molecules inside tissues can diffuse long enough that they are well mixed at the end of the saturation phase, all the distinct water compartments can be approximated as a single mixed one, and hence a single water relaxation rate may be sufficient to describe all water molecules in the APT models. If true, this can simplify the analysis of APT data from real biological tissues, and the previously reported R_1 correction methods based on two-pool models can be applied in clinical practice.

Unfortunately, the influences of multiple water pools, heterogeneous relaxation and transcytolemmal water exchange on CEST measurements have not previously been fully investigated. Therefore, in this study computer simulations and measurements *in vivo* were performed to evaluate such effects. Specifically, a more general four-pool model consisting of intracellular water, extracellular water, exchanging protons and an MT pool was examined using computer simulations. Furthermore, the hypothesis of relaxation influence and compensation was directly tested *in vivo*: tumor-bearing rats with regions of blood–brain-barrier breakdown received serial injections of Gd-DTPA while measuring CEST signals. By such a means, the extracellular water relaxation rate was selectively altered as tracked by R_1 mapping, and hence the effectiveness and accuracy of R_1 corrections were investigated. In addition to the R_1-corrected AREX contrast, the conventional MTR_{asym} and APT* metrics were also calculated and compared to quantify the influence of R_1 variations on APT contrast.

METHODS

Quantification of APT

For the simple two-pool (water and amide protons) model, the CEST effect is defined as a function of two Z-spectral values: the label scan $Z_{lab} = M_{lab}/M_0$, acquired at the amide proton frequency (3.6 ppm in biological tissues) and a reference scan Z_{ref} that has no contribution of amide. The conventional MTR_{asym} uses the

NMR IN BIOMEDICINE

opposite frequency as a reference scan $Z_{ref} = Z(-3.6$ ppm), acquired at the amide proton frequency (3,16), namely

$$\mathrm{MTR_{asym}(APT)} = Z_{ref}\text{-}Z_{lab} = Z(-3.6\mathrm{ppm}) - Z(3.6\mathrm{ppm}). \quad [1]$$

However, $Z(-3.6$ ppm) is contaminated by asymmetric MT and NOE effects in biological tissues. Jin *et al.* (16) found that Z-values at 3.0 and 4.2 ppm of rodent brain tissues at 9.4 T appeared to have minimal APT saturation effect, and hence defined the apparent APT contrast APT* using the three-offset method as

$$\mathrm{APT^*} = Z^*_{ref} - Z_{lab} = \frac{Z(3.0\,\mathrm{ppm}) + Z(4.2\,\mathrm{ppm})}{2} - Z(3.6\,\mathrm{ppm}). \quad [2]$$

Zaiss *et al.* defined the apparent exchange-dependent relaxation (AREX) using the $1/Z$ analysis as (19)

$$\mathrm{AREX(APT)} = \left(\frac{1}{Z_{lab}} - \frac{1}{Z_{ref}}\right)R_1 = \left(\frac{1}{Z(3.6\,\mathrm{ppm})} - \frac{1}{Z(-3.6\,\mathrm{ppm})}\right)R_1. \quad [3]$$

However, Equation [3] was derived based on a simple two-pool model without the consideration of other confounding effects, e.g. asymmetric MT and NOE, which may play an important role in biological tissues. Specifically, $Z_{ref}(-3.6$ ppm) may suffer contamination from these effects, which may bias the estimation of AREX(APT). To reduce these contaminations, we previously proposed to use Z^*_{ref} in the three-offset method to replace Z_{ref} and obtained (21,23)

$$\mathrm{AREX^*(APT)} = \left(\frac{1}{Z_{lab}} - \frac{1}{Z^*_{ref}}\right)R_1 = \left(\frac{1}{Z(3.6\,\mathrm{ppm})} - \frac{2}{Z(3.0\,\mathrm{ppm}) + Z(4.2\,\mathrm{ppm})}\right)R_1. \quad [4]$$

The detailed derivations of Equations [3] and [4] have been reported before (19,20,25), and have already been applied in previous studies (19,21,23,29). The quantity AREX* corrects for spillover, R_1 and asymmetric MT effects, and hence should provide an exchange-rate-weighted APT measurement relatively free of other influences (21). Note that, in principle, the AREX method is independent of how the reference value is obtained.

Numerical simulations

Numerical simulations based on a four-pool model were performed by solving Bloch–McConnell equations using scripts written in-house in MATLAB (MathWorks, Natick, MA, USA). The four pools were denoted as intracellular water (A), extracellular water (B), macromolecular MT (C), and amide (D) protons. Proton exchange was allowed between any two pools except that the amide (D) pool could only exchange with intracellular water (A). Note that a separate work found that distinct macromolecular pools exchanging with the intra and extra cellular water pools were not necessary when fitting quantitative MT data with rapid transcytolemmal exchange (30). Hence, we use only one macromolecular pool here. A schematic diagram with corresponding exchange rate constants is shown in Figure 1. The parameters

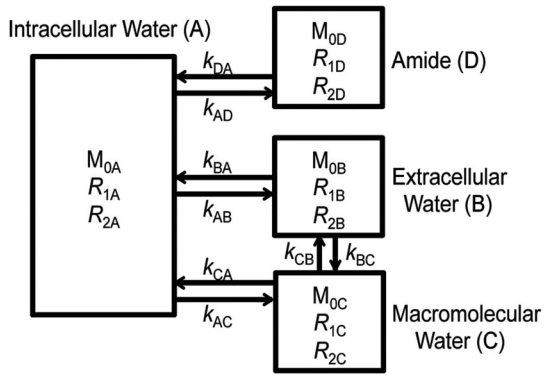

Figure 1. Schematic diagram of a four-pool model comprised of intracellular water (A), extracellular water (B), macromolecular water (C), and amide proton (D) pools. Arrows indicate possible magnetization exchanges between pools.

used in the simulations were (7,31) $M_{0A} = 0.6888$, $R_{1A} = 0.4$ s^{-1}, $R_{2A} = 20$ s^{-1}, $M_{0B} = 0.25$, $R_{2B} = 20$ s^{-1}, $M_{0C} = 0.06$, $R_{1C} = 1$ s^{-1}, $R_{2C} = 10^5$ s^{-1}, $M_{0D} = 0.0012$, $R_{1D} = 1$ s^{-1}, and $R_{2D} = 66.67$ s^{-1}, and the extracellular water R_{1B} varied from 0.3 to 3.3 s^{-1} to mimic the contrast-agent-induced R_1 variations from 0.4 to 1 Hz observed in the experiments *in vivo* (see Fig. 6 later). Other parameters were amide water exchange rate constant $k_{DA} = 30$ s^{-1}, macromolecular water exchange rate constant $k_{CA} = k_{CB} = 20$ s^{-1}, and transcytolemmal water exchange rate constant $k_{AB} = 0$, 1, 2, 4, or 6 s^{-1}. The observed R_1 of the whole system was simulated with a selective inversion recovery method as described previously (31–33). $\mathrm{MTR_{asym}}$, APT*, and AREX* were simulated and calculated according to Eqs. [1], [3] and [4]. The MR sequence parameters (T_R, T_E, RF duration, and power) were the same as those used in the *in vivo* experiments (see below).

MRI of animals

All animal-related procedures were approved by the Institutional Animal Care and Use Committee at Vanderbilt University. Six male Fisher 344 rats (280–310 g) bearing 9L brain tumors were scanned. MR images were acquired on a 9.4 T Varian 21 cm bore horizontal imaging system with a 38 mm RF volume coil for both transmission and reception. During MRI experiments, the rat rectal temperature was maintained at around 37 °C using a warm-air feedback system.

Figure 2(b) shows the *in vivo* experimental protocol of the current study. The intravenous injections of Gd-DTPA (0.083 mmol kg^{-1}) were repeated four times to obtain five (including the baseline) different accumulated Gd-DTPA concentrations as well as five different R_1 values. The measurements of B_0 field map, R_1, APT, and spoiled-gradient echo (SPGR) signals were interleaved and repeated five times to obtain multiple MR parametric maps with five different R_1 values. To assist in determining the delay time between each Gd-DTPA injection and each APT measurement, the SPGR sequence was used starting from 1 min before through 13 min after each Gd-DTPA injection to monitor the time course of R_1 variations caused by Gd-DTPA. Figure 2(a) shows the SPGR signals of the tumor (red squares) and contralateral normal brain tissue (blue circles) from a representative rat. The SPGR signals reached a relatively flat plateau after 13 min of Gd-DTPA injections, indicating that R_1 was relatively stable after that time. Therefore, except for the baseline,

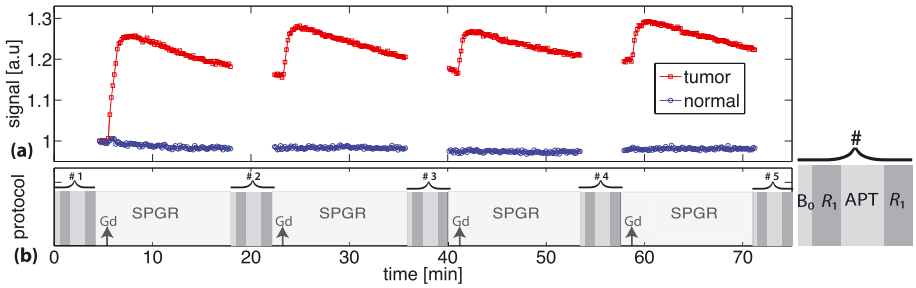

Figure 2. (a) Time course of SPGR signals of a tumor and contralateral normal brain tissue from a representative rat. (b) Schematic diagram of the data acquisition protocol. The acquisitions of B_0, R_1, APT, R_1, and SPGR signals were interleaved and repeated five times. The arrows indicate the times when Gd-DTPA was injected.

all the acquisitions of multiple MR parametric maps were performed after 13 min from each Gd-DTPA injection. By such a means, rapid variations of R_1 were avoided during all APT measurements. Furthermore, to quantify the R_1 changes, two R_1 maps were acquired immediately before and after each repeated APT measurement, respectively, and hence the percentage R_1 variation δR_1 ($\delta R_1\% = 200|R_{1\text{before}} - R_{1\text{after}}|/|R_{1\text{before}} + R_{1\text{after}}|$) can be obtained, showing the percentage R_1 change during each APT measurement. In order to monitor possible B_0 shifts during the whole experiments, a B_0 map was acquired before each of the five APT measurements.

Specifically, B_0 field maps were reconstructed from four complex gradient echo images with T_E = 3, 5, 7, and 9 ms. R_1 was mapped using a seven-point selective inversion recovery sequence specifically optimized for cancer imaging (30). APT measurements were acquired with 5 s continuous wave saturation pulses with B_1 = 1 μT. Five frequency offsets (300, 4.2, 3.6, 3, −3.6 ppm) were acquired in each APT measurement. Note that B_0 variations were monitored during experiments (see Fig. 4 later). R_1 and APT images were acquired on a single slice of 2 mm thickness using a single-shot spin-echo echo-planar imaging (EPI) sequence (field of view = 32 × 32 mm^2; matrix size = 64 × 64). After the pixel-wise mapping of B_0, R_1, MTR_{asym}, APT*, and AREX*, quantitative analyses were performed on regions of interest (ROIs) of the tumors and the corresponding contralateral normal tissues.

RESULTS

Numerical simulations

Figure 3 shows the simulated dependence of MTR_{asym}, APT*, and AREX* on the average R_1 for the four-pool model. The change of R_1 was achieved via adjusting R_{1b} of the extracellular water only, mimicking the effects of injections of Gd-DTPA. The transcytolemmal water exchange rate constant k_{AB} was allowed to vary from 0 to 6 Hz, with corresponding intracellular water lifetime from infinity to 167 ms. MTR_{asym} and APT* were very dependent on R_1 at all values of k_{AB}, e.g. about 41% change when R_1 changed from 0.4 to 1 Hz. The values from both methods are highly affected by R_1 no matter how fast the transcytolemmal water exchange is. By contrast, although the R_1-corrected AREX* showed slight variations (~10%) for $k_{AB} < 2$ Hz, it became relatively independent of R_1 (<5%) over a broad range of R_1 values from 0.4 to 1.2 Hz when transcytolemmal water exchange was faster ($k_{AB} > 2$ Hz). This suggests that R_1 effects can be eliminated from R_1-corrected AREX* if k_{AB} is fast enough. Even if k_{AB} is relatively slow (<2 Hz), the R_1 effects are still small (~10%) in AREX*. In contrast, both MTR_{asym} and APT* are significantly influenced (~40%) by R_1 effects even with large k_{AB} values.

In vivo MRI experiments

Figure 4 shows the δR_1 variation and B_0 field shift during the MRI scans of a representative animal. Recall that δR_1 is the percentage change of R_1 before and after each of the five APT measurements. Although δR_1 of the tumors increased slightly with the accumulation of injected Gd-DTPA, simulations indicated that the variations of APT* were less than 1% and the variations of MTR_{asym} less than 5% for $\delta R_1 < 3.5\%$ (data not shown). Thus the variations of R_1 that occurred during each APT measurement were ignored in the current study. Figure 4B shows that ΔB_0 was constant in both tumors and contralateral normal tissues throughout the whole experiments. Therefore, the B_0 field shift was not considered in the data analyses of the current study, since the maximum B_0 shift was only about 5 Hz (0.0125 ppm) in the ROIs.

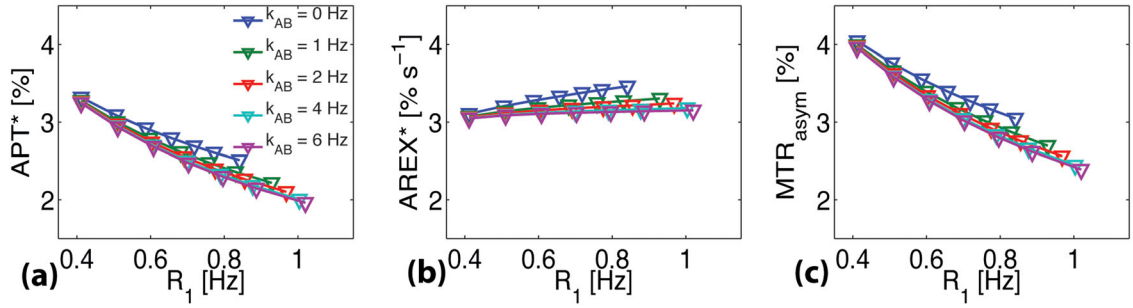

Figure 3. Simulated dependence of APT* (a), R_1-corrected AREX* (b), and MTR_{asym} (c) on R_1 with different transcytolemmal water exchange rate constants k_{AB}.

NMR IN BIOMEDICINE

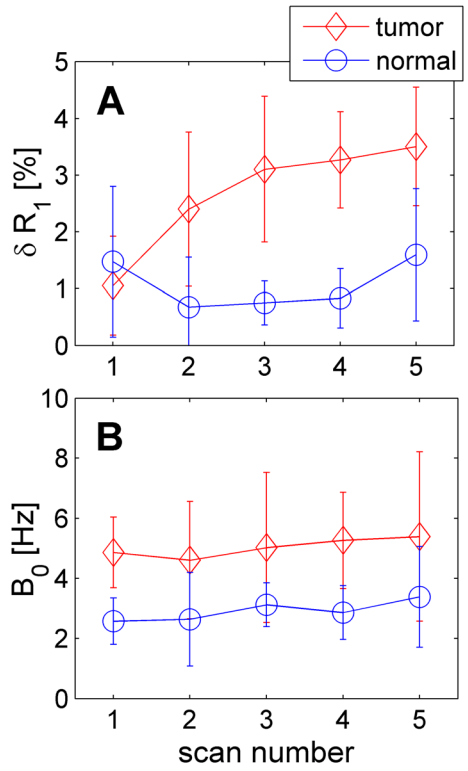

Figure 4. The δR_1 variation between before and after each repeated APT measurement (A) and B_0 field shift at the starting point of each APT measurement (B). Scan number represents the repeated scans, and Scan 1 represents the baseline acquisition

Figure 5 shows the multi-parametric maps of a representative rat brain for each of the dynamic scans. The R_1 maps confirm that the injections of Gd-DTPA affected the tumors only, as expected. The fifth R_1 map (top right) shows the ROIs manually selected on the tumor (green) and contralateral normal tissues (black). Consistent with the numerical simulations (see above), APT* values were lower in tumors after the Gd-DTPA injections. By contrast, MTR_{asym} in tumors increased gradually with Gd-DTPA injections, which is different from the predicted results that MTR_{asym} should decrease with higher R_1 values. This discrepancy may be due to other effects such as the presence of NOE contributions. The R_1-corrected AREX* was constant throughout all scans, indicating that it was independent of the R_1 variations caused by the Gd-DTPA injections.

Figure 6 summarizes the correlations between APT measures (APT*, AREX*, and MTR_{asym}) and R_1 obtained *in vivo*. For the tumors, APT* appears to be significantly inversely correlated with R_1 (Spearman's correlation $r = -0.795$ and $p < 0.001$), but R_1-corrected AREX* showed no significant correlation with R_1 ($p = 0.503$). Note also that, consistent with previous reports (21), R_1-corrected AREX* in tumors ($3.34 \pm 0.40\%\ s^{-1}$) is very similar to that in normal tissues ($3.33 \pm 0.35\%\ s^{-1}$). Although MTR_{asym} showed a slightly positive correlation with R_1 ($r = 0.477$), which is different from the stronger negative correlations predicted by the simulations, the dependence of MTR_{asym} on R_1 is clear ($p = 0.008$). The predicted decrease of MTR_{asym} with increasing R_1 agrees with previous simulations based on a simple two-pool model (water and amide) (34), but is at variance with the experimental results found here. This may be due to the influence of NOE effects that were not considered in the simulations or to differences between the parameter values used in the simulations and the actual values present *in vivo*. Nevertheless, these results confirm again that MTR_{asym} and APT* are significantly affected by R_1 values, and hence their accuracy for quantifying mobile proteins/peptides is compromised. By contrast, R_1-corrected AREX* is immune to the large variations of R_1 (from 0.4 to 1.0 Hz) in real tissues in which multiple water compartments exist. This suggests that R_1-corrected AREX* is a more reliable indicator of levels of mobile proteins/peptides than other APT methods. For reference, the correlations of APT values with R_1 in contralateral normal tissues are also provided in Figure 6.

DISCUSSION

In order to obtain reliable measurements of APT, it is necessary to remove or correct for possible influences other than chemical exchange with amides in mobile peptides and proteins. Effects such as the presence of asymmetric MT, variations in R_1, RF spillover, and NOEs can reduce the accuracy and specificity of APT in practice, and lessen its value as a molecular imaging technique. For example, any detected APT changes without corrections for confounding effects could be due to changes in R_1, MT, or amide proton concentrations, or combinations of these effects. This will

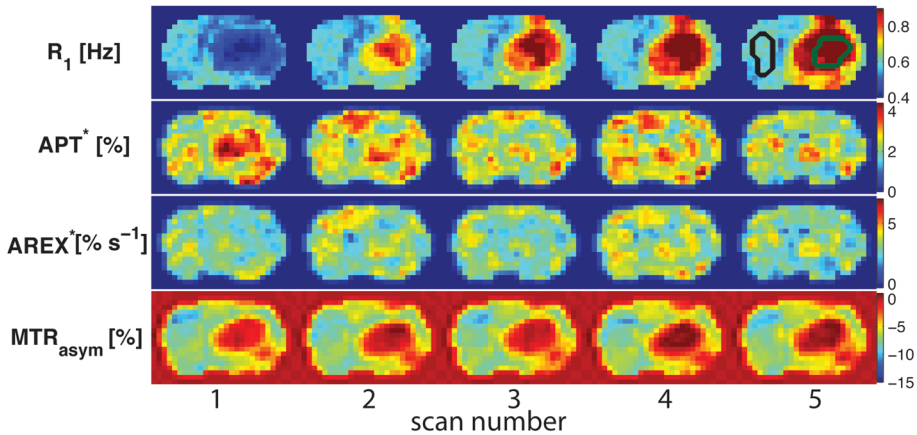

Figure 5. Temporal evolution of R_1, APT*, AREX*, and MTR_{asym} maps acquired from a representative rat before and after Gd-DTPA injections. The fifth R_1 map shows the ROIs of the tumor (green) and contralateral normal tissues (black) used in the data analysis.

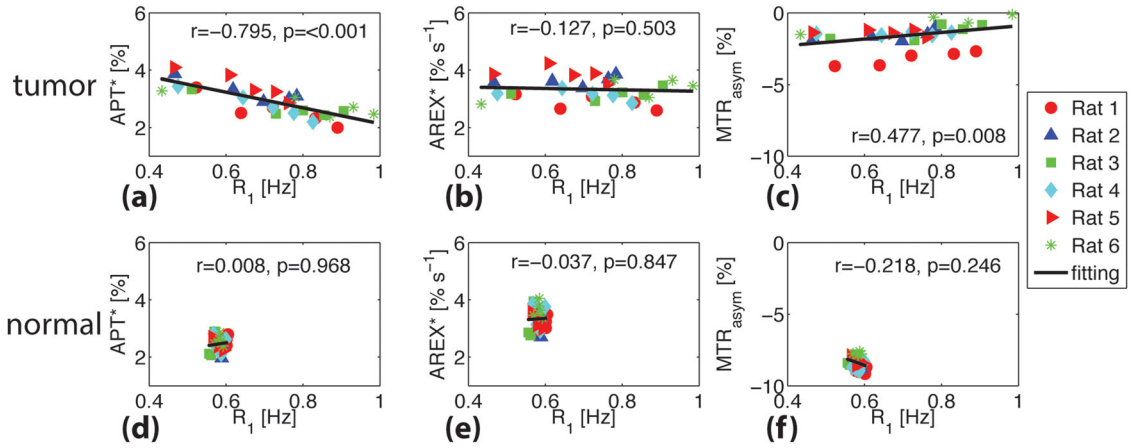

Figure 6. Correlations of tumor APT* (a), AREX* (b), and MTR_{asym} (c) with R_1 for six rats. The corresponding correlations for the contralateral normal brain tissues are shown in (d), (e), and (f) respectively. The Spearman's coefficient *r* and *p* values are provided for each correlation. The full lines represent the linear regression of all data points in each subfigure.

increase the difficulty of interpreting APT data and hinder its application in practice. We have previously proposed to use AREX* to correct other confounding effects and achieved a relatively "clean" exchange-rate-dependent metric. However, previous studies using AREX* are all based a simple two-pool model, and the accuracy in biological tissues with multiple physical compartments has not been fully investigated before. The current study aimed to evaluate whether the existence of multiple water compartments in real tissues with heterogeneous relaxation rates could affect the measurements of APT by different methods. The results suggest that both conventional MTR_{asym} and the three-offset APT* methods may be strongly affected by values of R_1, while R_1-corrected AREX* is independent of R_1 over a broad physiologically relevant range (0.4–1.0 Hz). This indicates that R_1 significantly confounds conventional APT measures; and the R_1-corrected AREX metric based on the $1/Z$ method is an appropriate means to remove R_1 influences on APT measurements.

Note that, after a single bolus injection of Gd-DTPA, tumor R_1 could change significantly during the wash-in and wash-out processes. However, such a R_1 change is too fast for APT measurements, especially in the first 10 min or so after an injection. Although R_1 values were very different between different APT measurements in the current study, R_1 should be relatively stable during the acquisition of each APT measurement. Otherwise, the different R_1 weightings, e.g. at control and label scans, may cause a significantly biased estimation of APT. The same strategy has been used to map water exchange rates using multiple bolus injections of contrast agents (35). Therefore, APT measurements were made only when R_1 changes reached a relatively flat plateau (after 13 min) in the current study. Moreover, R_1 mapping was performed immediately before and after each APT measurement in order to confirm a relatively stable R_1 change during each APT measurement. Our simulations showed that the variations of APT* were less than 1% and the variations of MTR_{asym} less than 5% for $\delta R_1 < 3.5\%$ during each APT measurement.

A smaller value of R_1 implies a slower recovery from saturation, which should result in a larger value of MTR_{asym} (34). However, the observed MTR_{asym} in tumors showed a slight increase with increase of R_1. In biological tissues, MTR_{asym} may also be strongly affected by asymmetric MT and NOE effects. MTR_{asym} can be approximated as APTR – NOER, where APTR is the proton transfer ratio for the amide protons and NOER is the NOE-based MT ratio (36). Both APTR and NOER should decrease with increasing R_1, but the slight increase of MTR_{asym} with R_1 may suggest a stronger dependence of NOER on R_1 than APTR. In addition, the variation of R_1 during the acquisitions of APT images can also slightly bias the dependence of MTR_{asym} on R_1 (~5% shown in simulations). A different study also observed that MTR_{asym} changed significantly after Gd administration to patients who were to undergo carotid endarterectomy (37). This suggests that MTR_{asym} is not a reliable measure of mobile proteins/peptides and may be significantly affected by variations in R_1.

The apparent dependence of APT* and independence of AREX* on R_1 demonstrates the importance of R_1 corrections for interpreting APT changes. In our previous studies, it was shown that corrections for RF spillover, MT, and R_1 effects contributed differently in tumors (21) and stroke (23). APT* in tumors was higher than that in normal tissues, while R_1-corrected AREX* was similar in tumors and normal tissues (21), which was consistent with an independent study using a different approach (38). However, R_1-corrected AREX* showed a more pronounced contrast between ischemic and normal brain than APT* (23). Thus R_1 corrections may strongly affect inferences about changes within tissues in pathological conditions. Note that, although AREX* significantly reduces the contrast between brain tumors and normal brain tissues, it provides unique information on mobile proteins/peptides that are not achievable by other conventional MRI methods. Moreover, considering the potentially strong influence of other variables on APT measurements, other MR parameters (R_1, R_2, quantitative MT (e.g. the pool size ratio of macromolecular versus water protons)) should be measured to avoid misinterpretation of APT variations.

The amide proton pool is usually believed to be mainly within the intracellular space (7), so in our simulations we considered APT only between amide protons and intracellular water. However, the situation when both intra- and extracellular water protons exchange with amide protons has also been simulated, and the conclusion is qualitatively the same (specific data not shown): APT* and MTR_{asym} decreases with increasing R_1, but AREX* stays almost constant.

Both simulations and experiments show that R_1-corrected AREX* is independent of R_1. The intracellular exchange lifetime is much shorter than the total duration of saturation pulse(s) used in APT imaging (e.g. 5 s in the current study). The integrated water signal from all compartments may then be approximately regarded as from a single water pool. Therefore, though Gd-DTPA selectively alters the extracellular water R_1, the overall observed R_1 is still suitable for R_1 correction of APT imaging in biological tissues. Note that this conclusion may also hold for other exchange sites, e.g. amine. Therefore, under the circumstances when intracellular water lifetime is much shorter than the total duration of saturation pulse(s), i.e. fast transcytolemmal water exchange rate, the influences of different water compartmentation (i.e. intra- and extracellular spaces) and relaxation properties can be ignored because all water molecules can be considered well mixed at the end of the saturation pulse(s). This may assist better data interpretation of not only APT but also other types of CEST measurement.

The present work not only represents a verification of the proposed relaxation-compensated features of the APT evaluation method AREX*, but also has practical implications. Gadolinium-based contrast agents have been widely used in clinical MRI. However, due to their strong influence on R_1 relaxation, CEST measurements were not recommended with gadolinium injections (37). The current study shows that R_1-corrected AREX* can compensate the influences caused by variations in R_1 relaxation, and hence can be measured anytime, including after gadolinium injections. This can not only increase the accuracy of APT imaging when contrast agent is present, but also increase the management flexibility of patient imaging in clinical practice.

CONCLUSION

The effectiveness and accuracy of R_1 correction in APT imaging has been investigated via simulations and *in vivo* experiments. The time courses of APT*, MTR_{asym}, and AREX* were measured in tumors following serial injections of Gd-DTPA to result in different R_1 values. Different from conventional APT* and MTR_{asym} contrasts, R_1-corrected AREX* was found to be independent of R_1 changes. This study establishes the importance of R_1 corrections for accurate APT imaging, and confirmed the reliability of using the overall observed tissue R_1 for R_1 correction *in vivo*. Our results suggest an appropriate means to correct for R_1 and MT effects in CEST imaging, and may also assist in better understanding the contrast mechanisms of CEST imaging in biological tissues.

Acknowledgements

This work was funded by National Institutes of Health (NIH) K25CA168936, R01CA109106, R01CA173593, R01EB000214, P50CA128323, R21EB017873, R01EB017767, and R01CA184693.

REFERENCES

1. Ward KM, Aletras AH, Balaban RS. A new class of contrast agents for MRI based on proton chemical exchange dependent saturation transfer (CEST). J. Magn. Reson. 2000; 143: 79–87.
2. Van Zijl PCM, Yadav NN. Chemical exchange saturation transfer (CEST): what is in a name and what isn't? Magn. Reson. Med. 2011; 65: 927–948.
3. Zhou J, Lal B, Wilson DA, Laterra J, van Zijl PC. Amide proton transfer (APT) contrast for imaging of brain tumors. Magn. Reson. Med. 2003; 50: 1120–1126.
4. Jones CK, Schlosser MJ, Van Zijl PCM, Pomper MG, Golay X, Zhou J. Amide proton transfer imaging of human brain tumors at 3T. Magn. Reson. Med. 2006; 56: 585–592.
5. Salhotra A, Lal B, Laterra J. Amide proton transfer imaging of 9L gliosarcoma and human glioblastoma xenografts. NMR Biomed. 2008; 21: 489–497.
6. Jia G, Abaza R, Williams JD, Zynger DL, Zhou J, Shah ZK, Patel M, Sammet S, Wei L, Bahnson RR, Knopp MV. Amide proton transfer MR imaging of prostate cancer: a preliminary study. J. Magn. Reson. Imaging 2011; 33: 647–654.
7. Zhou J, Payen J-F, Wilson DA, Traystman RJ, van Zijl PCM. Using the amide proton signals of intracellular proteins and peptides to detect pH effects in MRI. Nat. Med. 2003; 9: 1085–1090.
8. Jokivarsi KT, Gröhn HI, Gröhn OH, Kauppinen RA. Proton transfer ratio, lactate, and intracellular pH in acute cerebral ischemia. Magn. Reson. Med. 2007; 57: 647–653.
9. Sun PZ, Zhou J, Huang J, Van Zijl P. Simplified quantitative description of amide proton transfer (APT) imaging during acute ischemia. Magn. Reson. Med. 2007; 57: 405–410.
10. Sun PZ, Zhou J, Sun W, Huang J, van Zijl PCM. Detection of the ischemic penumbra using pH-weighted MRI. J. Cereb. Blood Flow Metab. 2007; 27: 1129–1136.
11. Kim M, Gillen J, Landman BA, Zhou J, van Zijl PC. Water saturation shift referencing (WASSR) for chemical exchange saturation transfer (CEST) experiments. Magn. Reson. Med. 2009; 61: 1441–1450.
12. Lee JS, Regatte RR, Jerschow A. Isolating chemical exchange saturation transfer contrast from magnetization transfer asymmetry under two-frequency rf irradiation. J. Magn. Reson. 2011; 215: 56–63.
13. Scheidegger R, Vinogradov E, Alsop DC. Amide proton transfer imaging with improved robustness to magnetic field inhomogeneity and magnetization transfer asymmetry using saturation with frequency alternating RF irradiation. Magn. Reson. Med. 2011; 66: 1275–1285.
14. Zu Z, Xu J, Li H, Chekmenev EY, Quarles CC, Does MD, Gore JC, Gochberg DF. Imaging amide proton transfer and nuclear overhauser enhancement using chemical exchange rotation transfer (CERT). Magn. Reson. Med. 2014; 72: 471–476.
15. Xu J, Yadav NN, Bar-Shir A, Jones CK, Chan KWY, Zhang J, Walczak P, McMahon MT, Van Zijl PCM. Variable delay multi-pulse train for fast chemical exchange saturation transfer and relayed-nuclear overhauser enhancement MRI. Magn. Reson. Med. 2014; 71: 1798–1812.
16. Jin T, Wang P, Zong X, Kim SG. MR imaging of the amide-proton transfer effect and the pH-insensitive nuclear Overhauser effect at 9.4 T. Magn. Reson. Med. 2013; 69: 760–770.
17. Zu Z, Janve VA, Xu J, Does MD, Gore JC, Gochberg DF. A new method for detecting exchanging amide protons using chemical exchange rotation transfer. Magn. Reson. Med. 2013; 69: 637–647.
18. Zaiss M, Bachert P. Exchange-dependent relaxation in the rotating frame for slow and intermediate exchange – modeling off-resonant spin-lock and chemical exchange saturation transfer. NMR Biomed. 2013; 26: 507–518.
19. Zaiss M, Xu J, Goerke S, Khan IS, Singer RJ, Gore JC, Gochberg DF, Bachert P. Inverse *Z*-spectrum analysis for spillover-, MT-, and T_1-corrected steady-state pulsed CEST-MRI – application to pH-weighted MRI of acute stroke. NMR Biomed. 2014; 27: 240–252.
20. Zaiss M, Bachert P. Chemical exchange saturation transfer (CEST) and MR *Z*-spectroscopy *in vivo*: a review of theoretical approaches and methods. Phys. Med. Biol. 2013; 58: R221–269.
21. Xu J, Zaiss M, Zu Z, Li H, Xie J, Gochberg DF, Bachert P, Gore JC. On the origins of chemical exchange saturation transfer (CEST) contrast in tumors at 9.4 T. NMR Biomed. 2014; 27: 406–416.
22. Zaiss M, Windschuh J, Paech D, Meissner JE, Burth S, Schmitt B, Kickingereder P, Wiestler B, Wick W, Bendszus M, Schlemmer HP, Ladd ME, Bachert P, Radbruch A. Relaxation-compensated CEST-MRI of the human brain at 7 T: unbiased insight into NOE and amide signal changes in human glioblastoma. Neuroimage 2015; 112: 180–188.
23. Li H, Zu Z, Zaiss M, Khan IS, Singer RJ, Gochberg DF, Bachert P, Gore JC, Xu J. Imaging of amide proton transfer and nuclear Overhauser enhancement in ischemic stroke with corrections for competing effects. NMR Biomed. 2015; 28: 200–209.
24. Sun PZ, Wang E, Cheung JS. Imaging acute ischemic tissue acidosis with pH-sensitive endogenous amide proton transfer (APT) MRI – correction of tissue relaxation and concomitant RF irradiation effects

toward mapping quantitative cerebral tissue pH. Neuroimage 2012; 60: 1–6.
25. Zaiss M, Zu Z, Xu J, Schuenke P, Gochberg DF, Gore JC, Ladd ME, Bachert P. A combined analytical solution for chemical exchange saturation transfer and semi-solid magnetization transfer. NMR Biomed. 2015; 28: 217–230.
26. Syková E, Svoboda J, Polák J, Chvátal A. Extracellular volume fraction and diffusion characteristics during progressive ischemia and terminal anoxia in the spinal cord of the rat. J. Cereb. Blood Flow Metab. 1994; 14: 301–311.
27. Nilsson M, Lätt J, van Westen D, Brockstedt S, Lasič S, Ståhlberg F, Topgaard D. Noninvasive mapping of water diffusional exchange in the human brain using filter-exchange imaging. Magn. Reson. Med. 2013; 69: 1573–1581.
28. Bailey C, Giles A, Czarnota GJ, Stanisz GJ. Detection of apoptotic cell death in vitro in the presence of Gd-DTPA-BMA. Magn. Reson. Med. 2009; 62: 46–55.
29. Wu R, Xiao G, Zhou IY, Ran C, Sun PZ. Quantitative chemical exchange saturation transfer (qCEST) MRI – RF spillover effect-corrected omega plot for simultaneous determination of labile proton fraction ratio and exchange rate. NMR Biomed. 2015; 28: 376–383.
30. Li K, Li H, Zhang X, Stokes AM, Kang H, Zu Z, Quarles CC, Gochberg DF, Gore JC, Xu J. Influence of water compartmentation and heterogeneous relaxation on quantitative magnetization transfer imaging in rodent brain tumors. Magn. Reson. Med. 2015. DOI: 10.1002/mrm.25893 [Epub ahead of print].
31. Xu J, Li K, Zu Z, Li X, Gochberg DF, Gore JC. Quantitative magnetization transfer imaging of rodent glioma using selective inversion recovery. NMR Biomed. 2014; 27: 253–260.
32. Li K, Zu Z, Xu J, Janve VA, Gore JC, Does MD, Gochberg DF. Optimized inversion recovery sequences for quantitative T_1 and magnetization transfer imaging. Magn. Reson. Med. 2010; 64: 491–500.
33. Gochberg DF, Gore JC. Quantitative imaging of magnetization transfer using an inversion recovery sequence. Magn. Reson. Med. 2003; 49: 501–505.
34. Liu G, Song X, Chan KWY, Mcmahon MT. Nuts and bolts of chemical exchange saturation transfer MRI. NMR Biomed. 2013; 26: 810–828.
35. Bailey C, Moosvi F, Stanisz GJ. Mapping water exchange rates in rat tumor xenografts using the late-stage uptake following bolus injections of contrast agent. Magn. Reson. Med. 2013; 71: 1874–1887.
36. Zhou J, Hong X, Zhao X, Gao JH, Yuan J. APT-weighted and NOE-weighted image contrasts in glioma with different RF saturation powers based on magnetization transfer ratio asymmetry analyses. Magn. Reson. Med. 2013; 70: 320–327.
37. Tee YK, Donahue MJ, Harston GWJ, Payne SJ, Chappell MA. Quantification of amide proton transfer effect pre- and post-gadolinium contrast agent administration. J. Magn. Reson. Imaging 2014; 40: 832–838.
38. Scheidegger R, Wong ET, Alsop DC. Contributors to contrast between glioma and brain tissue in chemical exchange saturation transfer sensitive imaging at 3 Tesla. Neuroimage 2014; 99: 256–268.
39. Morrison C, Stanisz G, Henkelman RM. Modeling magnetization transfer for biological-like systems using a semi-solid pool with a super-Lorentzian lineshape and dipolar reservoir. J. Magn. Reson. B 1995; 108: 103–113.

APPENDIX

A detailed description of the four-pool model (see Fig. 1) and parameters has been presented in the text. The corresponding modified Bloch–McConnell equations including the transcytolemmal exchange between the intra- and extracellular compartments can be expressed as

$$\frac{d}{dt}\begin{bmatrix} M_{xA} \\ M_{yA} \\ M_{zA} \\ M_{zC} \\ M_{xB} \\ M_{yB} \\ M_{zB} \\ M_{xD} \\ M_{yD} \\ M_{zD} \end{bmatrix} = \begin{bmatrix} -r_{2A} & -\Delta\omega & 0 & 0 & k_{BA} & 0 & 0 & k_{DA} & 0 & 0 \\ \Delta\omega & -r_{2A} & \omega_1 & 0 & 0 & k_{BA} & 0 & 0 & k_{DA} & 0 \\ 0 & -\omega_1 & -r_{1A} & k_{CA} & 0 & 0 & k_{BA} & 0 & 0 & k_{DA} \\ 0 & 0 & k_{AC} & -r_{1C} & 0 & 0 & 0 & 0 & 0 & 0 \\ k_{AB} & 0 & 0 & 0 & -r_{2B} & -\Delta\omega & 0 & 0 & 0 & 0 \\ 0 & k_{AB} & 0 & 0 & \Delta\omega & -r_{2B} & 0 & 0 & 0 & 0 \\ 0 & 0 & k_{AB} & 0 & 0 & 0 & -r_{1B} & 0 & 0 & 0 \\ k_{AD} & 0 & 0 & 0 & 0 & 0 & 0 & -r_{2D} & -\Delta\omega & 0 \\ 0 & k_{AD} & 0 & 0 & 0 & 0 & 0 & \Delta\omega & -r_{2D} & 0 \\ 0 & 0 & k_{AD} & 0 & 0 & 0 & 0 & 0 & 0 & -r_{1D} \end{bmatrix} + \begin{bmatrix} 0 \\ 0 \\ R_{1A}M_{0A} \\ R_{1C}M_{0C} \\ 0 \\ 0 \\ R_{1B}M_{0B} \\ 0 \\ 0 \\ R_{1D}M_{0D} \end{bmatrix} \quad \text{(S1)}$$

with $r_{2A} = R_{2A} + k_{AB} + k_{AD}$, $r_{1A} = R_{1A} + k_{AB} + k_{AC} + k_{AD}$, $r_{1C} = R_{1C} + k_{CA} + R_{RFB,C}$, $r_{2B} = R_{2B} + k_{BA}$, $r_{1B} = R_{1B} + k_{BA}$, $r_{2D} = R_{2D} + k_{DA}$, and $r_{1D} = R_{1D} + k_{DA}$, where $R_{RFB} = \pi\omega_1^2 g(2\pi\Delta)$ is the saturation rate of the macromolecular pool, and g is the super-Lorentzian lineshape (39)

$$g(2\pi\Delta) = \sqrt{\frac{2}{\pi}} T_{2B} \int_0^1 \frac{1}{|3u^2 - 1|} e^{-2\left(\frac{2\pi\Delta T_{2B}}{3u^2-1}\right)^2} du \quad \text{(S2)}$$

where T_{2B} is the transverse relaxation time of the macromolecular protons and Δ is the frequency offset. Note that only continuous-wave APT experiments were considered in the current study, so Equation [S1] was directly adopted and matrix operations were performed to simulate the signals. All simulations were based on scripts written in-house with MATLAB (MathWorks, Natick, MA, USA). It took about 4 s on an i5-3210M 2.5 GHz processor to complete one set of simulations (i.e. 4 k_{AB} values, 14 R_1 values, and 121 frequency offsets).